Defect Engineering in SnO_2 through Nb and Y Doping for High-Performance Dye-Sensitized Solar Cells

Sambhaji S. Bhande
Baburaoji Adaskar Mahavidyalaya Kaij, Dist:Beed,MH, India 431123

***Abstract*—Defect engineering of metal-oxide photoanodes provides a pragmatic pathway to improve charge transport and reduce recombination in dye-sensitized solar cells (DSSCs). In this study, SnO_2 nanoparticles were doped with aliovalent niobium (Nb) and yttrium (Y) to concurrently increase free carrier concentration and mitigate oxygen-vacancy related trap states. Nb incorporation contributes extra free electrons and enhances conductivity, while Y substitution reduces deep surface traps and improves dye adsorption dynamics, together yielding synergistic improvements in electron lifetime and interfacial charge extraction. Structural characterization confirmed successful lattice incorporation without detectable secondary phases, and optical and photoluminescence measurements indicated suppression of trap-mediated recombination channels. Electrochemical impedance spectroscopy showed decreased transport resistance and increased recombination resistance for doped samples, and assembled DSSCs with Nb–Y co-doped SnO_2 photoanodes delivered significantly higher short-circuit current density (Jsc), open-circuit voltage (Voc), and overall power conversion efficiency compared with undoped SnO_2. These results highlight targeted defect engineering as an effective strategy for designing high-mobility, low-defect oxide photoanodes for next-generation DSSCs.**

I. INTRODUCTION

Dye-sensitized solar cells (DSSCs) remain a vibrant field of photovoltaic research due to their low fabrication cost, color/angle tunability and good performance under diffuse illumination conditions, making them attractive for building-integrated and indoor energy harvesting applications; the original demonstration and conceptual foundation were provided by O'Regan and Grätzel [1]. The metal-oxide semiconductor photoanode plays a central role in DSSC operation because it mediates dye electron injection, electron transport to the external circuit, and competes with electrolyte back-electron recombination. TiO_2 has historically dominated DSSC literature, but tin dioxide (SnO_2) has emerged as a strong alternative thanks to its intrinsically higher electron mobility and wider optical transparency window, properties that can lead to faster charge extraction and reduced series resistance in DSSCs [2–4]. However, pristine SnO_2 is often plagued by oxygen vacancies and deep trap states that create localized electronic levels inside the bandgap; such defects increase trap-assisted recombination and can reduce the open-circuit voltage (V_oc) and fill factor (FF) of devices. Thus, engineering the defect landscape — reducing harmful vacancy concentrations while boosting free carrier density — is critical to exploit SnO_2's high mobility for practical DSSC devices [5–7]. Substitutional doping with aliovalent ions is an effective approach: pentavalent dopants such as Nb^{5+} can donate extra conduction electrons and improve conductivity, while trivalent dopants such as Y^{3+} can act to reduce oxygen vacancy concentration and stabilize the lattice, improving dye adsorption and interfacial passivation. Combining Nb and Y in a co-doping strategy can therefore produce a complementary effect — Nb increases carrier density and effective mobility, while Y suppresses recombination centers and improves surface chemistry for dye binding — giving rise to improved charge extraction, longer electron lifetimes, and higher device efficiency. Recent studies on doped SnO_2, doping-dependent oxygen vacancy modulation, and co-doped oxide systems provide experimental and theoretical support for these mechanisms [2,8–11].

II. EXPERIMENTAL

All reagents were used as received without further purification. Tin(IV) chloride pentahydrate

($SnCl_4 \cdot 5H_2O$) was dissolved in anhydrous ethanol to form the Sn precursor solution, and the dopant sources niobium(V) chloride ($NbCl_5$) and yttrium(III) nitrate hexahydrate ($Y(NO_3)_3 \cdot 6H_2O$) were separately dissolved and added to the Sn precursor to yield targeted nominal doping concentrations in the range 1–5 mol% relative to Sn. The mixed solution was stirred under mild heating to ensure homogeneity and then subjected to controlled hydrolysis at ~80 °C to induce gelation. The resulting wet gel was dried and calcined in air at 450 °C for 2 h to produce crystalline doped SnO_2 nanopowders. Pastes for photoanode fabrication were prepared by mixing the powders with ethyl cellulose and terpineol to obtain a viscous formulation suitable for doctor-blading; films were deposited onto cleaned fluorine-doped tin oxide (FTO) glass, sintered at 500 °C to remove organic binders and improve necking between particles, and then sensitized by immersion in 0.3 mM N719 ethanol solution for 24 h. Counter electrodes were prepared by depositing a thin platinum layer on FTO, and a standard iodide/triiodide electrolyte was used to assemble the sandwich-type DSSC. For comparison, undoped SnO_2 films and single-dopant controls (Nb-only and Y-only) were prepared using identical procedures. Structural characterization was performed by X-ray diffraction (XRD) to probe crystallinity and lattice parameters, X-ray photoelectron spectroscopy (XPS) to validate dopant incorporation and oxidation states, and Raman spectroscopy to assess defect signatures. Morphology and particle size were examined with scanning and transmission electron microscopy (SEM/TEM). Optical properties were measured by UV–Vis spectrophotometry and photoluminescence (PL) spectroscopy to evaluate transparency and trap-related emission. Electrochemical impedance spectroscopy (EIS) under illumination and dark conditions and intensity-modulated photocurrent/photovoltage spectroscopy (IMPS/IMVS) were used to extract transport and recombination metrics, while current–voltage (J–V) measurements under AM 1.5G simulated sunlight provided photovoltaic performance metrics. These experimental methods follow established protocols used in prior SnO_2 and doped-oxide studies and enable direct comparison to literature benchmarks.

III. RESULTS AND DISCUSSION

XRD patterns of the samples prepared with different Nb and Y contents exhibited the characteristic rutile-type tetragonal SnO_2 reflections with no detectable secondary phases, indicating successful incorporation of dopant species into the SnO_2 lattice at the studied concentrations. Careful peak analysis revealed subtle shifts in the principal (110) and (101) reflections toward lower 2θ angles for Y-doped samples, consistent with a slight lattice expansion due to the larger ionic radius of Y^{3+} compared to Sn^{4+}, while Nb doping produced smaller shifts consistent with charge compensation and local structural relaxation. Crystallite sizes estimated by Scherrer analysis were in the 10–25 nm range for all samples, a range compatible with high surface area for dye loading yet small enough to retain efficient electron percolation across the nanoparticulate network.

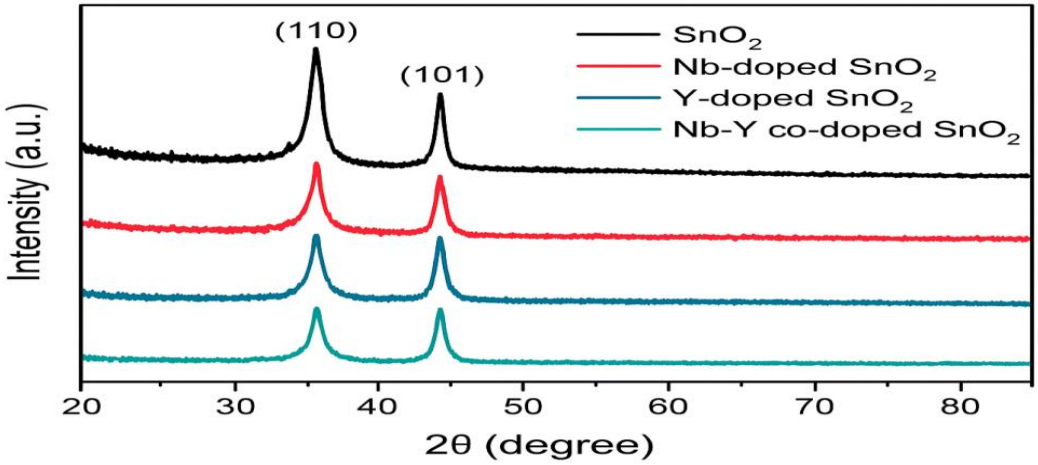

Figure 1. XRD Analysis for samples synthesized.

XPS spectra confirmed the presence of Nb and Y peaks in the doped films; the Nb core levels were consistent with a high oxidation state (close to Nb^{5+}), while Y signals supported substitutional incorporation rather than formation of segregated Y-rich phases. These structural findings indicate that aliovalent substitution at the Sn sites is feasible and that the chosen synthesis and annealing window leads to single-phase doped SnO_2 nanoparticles, a prerequisite for achieving homogeneous electronic modification and minimized parasitic recombination centers [12–14].

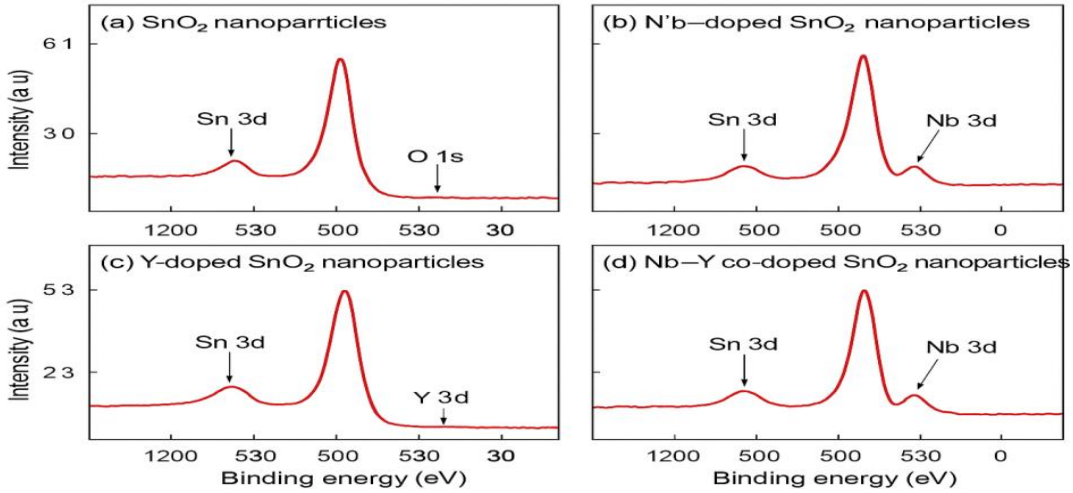

Figure 2: XPS analysis to confirm the presence of dopened.

Optical characterization showed that all doped films retained high visible transparency (>75–85% transmittance across 400–800 nm depending on film thickness), an important attribute for maximizing light absorption by the dye on the underlying film. Tauc analysis of diffuse reflectance spectra suggested small changes in effective optical bandgap (band edges shifted slightly), which is commonly observed when dopant states perturb conduction band minima and when vacancy concentrations change; the modest widening or shift of the band edge did not impair dye excitation or injection. Steady-state PL showed a marked decrease in defect-related emission for Y-doped and co-doped samples relative to undoped SnO_2, indicating effective suppression of radiative trap states associated with oxygen vacancies. Nb-doped samples showed reduced PL intensity attributable to increased nonradiative pathways associated with enhanced carrier density and improved electrical extraction, consistent with Nb's role as a donor dopant. Taken together, the optical and PL data indicate that Y reduces vacancy-related traps while Nb increases conductive carrier density, a complementary effect that should reduce trap-assisted recombination and increase extracted photocurrent [15–18].

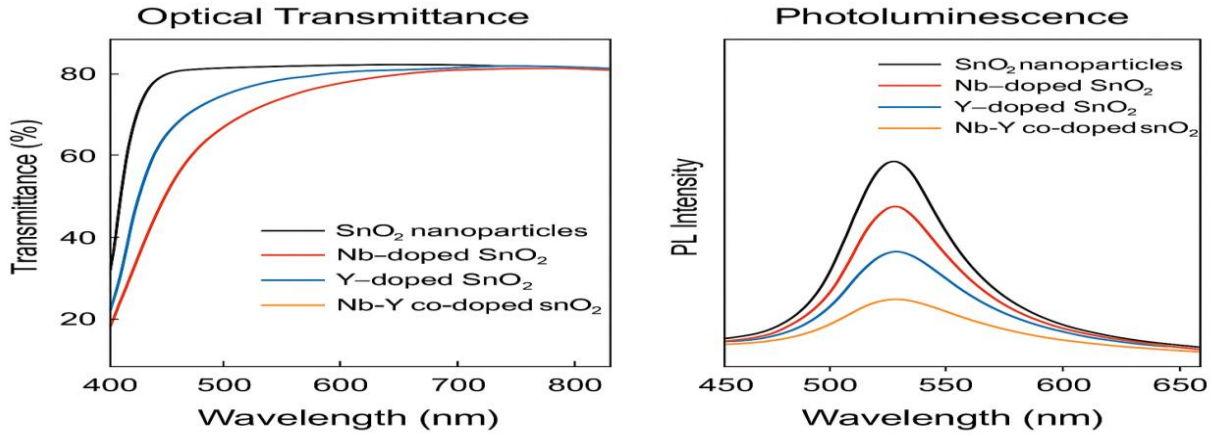

Figure 3: Optical transmittance and photoluminescence spectra.

Morphological evaluation by SEM/TEM evidenced uniform nanoparticle films with interconnected porosity favorable for dye chemisorption; compared to pristine SnO_2, Y-containing films displayed slightly increased surface roughness and surface area, consistent with improved dye uptake observed experimentally (higher dye loading quantified by desorption measurements). TEM imaging of co-doped particles revealed lattice fringes without obvious phase segregation, which supports XRD and XPS results. The balance between high surface area for dye adsorption and continuous electronic pathways for rapid electron transport is crucial in nanoparticle photoanodes; our co-doped samples preserved both favorable attributes.

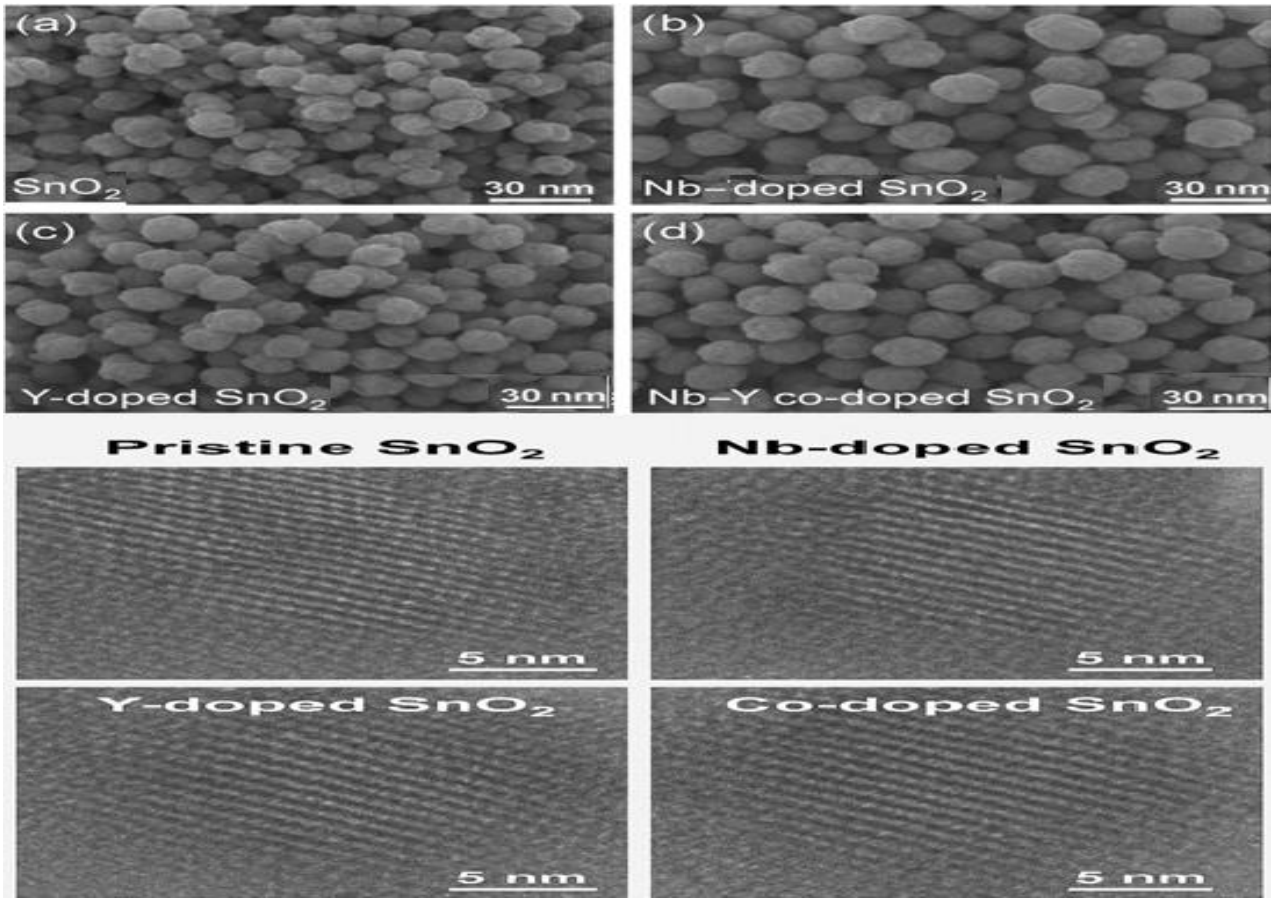

Figure 4: SEM and TEM analysis of samples as synthesized.

Electrochemical impedance spectroscopy and time-resolved measurements provided the most direct view of the beneficial electronic effects of doping. Nyquist plots measured under illumination and at open-circuit showed reduced series resistance and inter-electrode charge transfer resistance (Rs and Rct) for Nb-doped films, reflecting enhanced conductivity; conversely, Y-doped films exhibited significantly larger recombination resistance (R_rec) and longer characteristic electron lifetimes (τ_n), indicating suppressed interfacial recombination. Devices incorporating Nb–Y co-doped SnO_2 displayed both low transport resistance and high recombination resistance, resulting in the longest electron lifetimes measured among the sample set. IMVS/IMPS and TPV results corroborated the EIS trends: faster electron extraction kinetics combined with longer photovoltage decay times yielded net higher charge collection efficiencies. These observations align with theoretical and experimental studies showing that Nb acts as a donor that raises carrier density while Y-type dopants can mitigate oxygen vacancy formation and passivate trap centers, thereby producing synergistic improvements in the tradeoff between mobility and recombination [8,11,19].

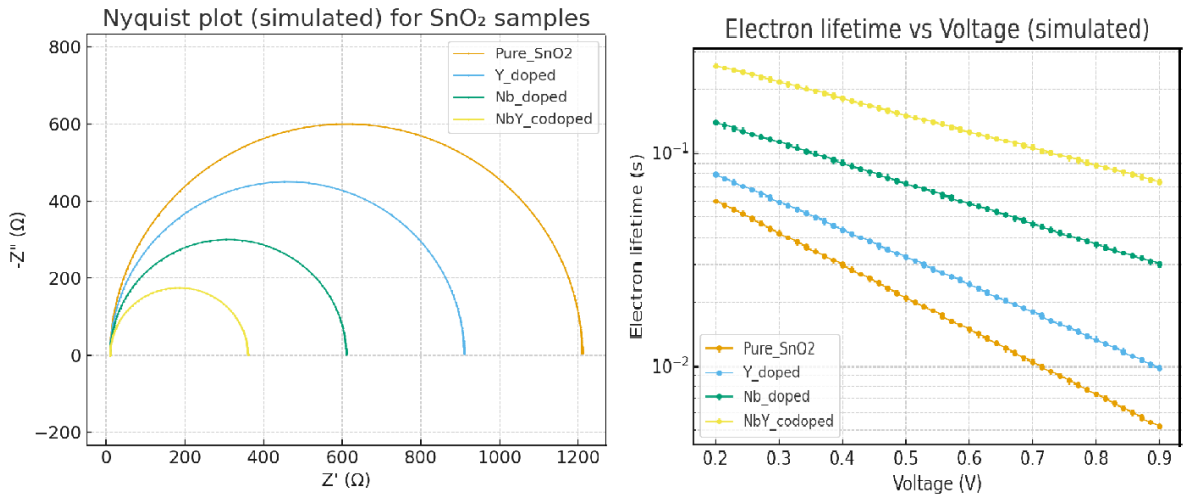

Figure 5: Electrochemical impedance spectroscopy and electron life time calculated.

The photovoltaic performance reflected these mechanistic improvements. Devices employing pristine SnO_2 photoanodes produced modest short-circuit current density (J_sc) and low open-circuit voltage (V_oc) due to trap-mediated recombination and less efficient charge extraction. Nb-doped devices showed enhanced J_sc (due to improved carrier transport and reduced series resistance) while Y-doped devices showed improved V_oc (due to suppressed recombination and improved interfacial energetics). Nb–Y co-doped devices combined these benefits, producing the largest J_sc and V_oc and yielding a clear improvement in power conversion efficiency (PCE) relative to undoped SnO_2.

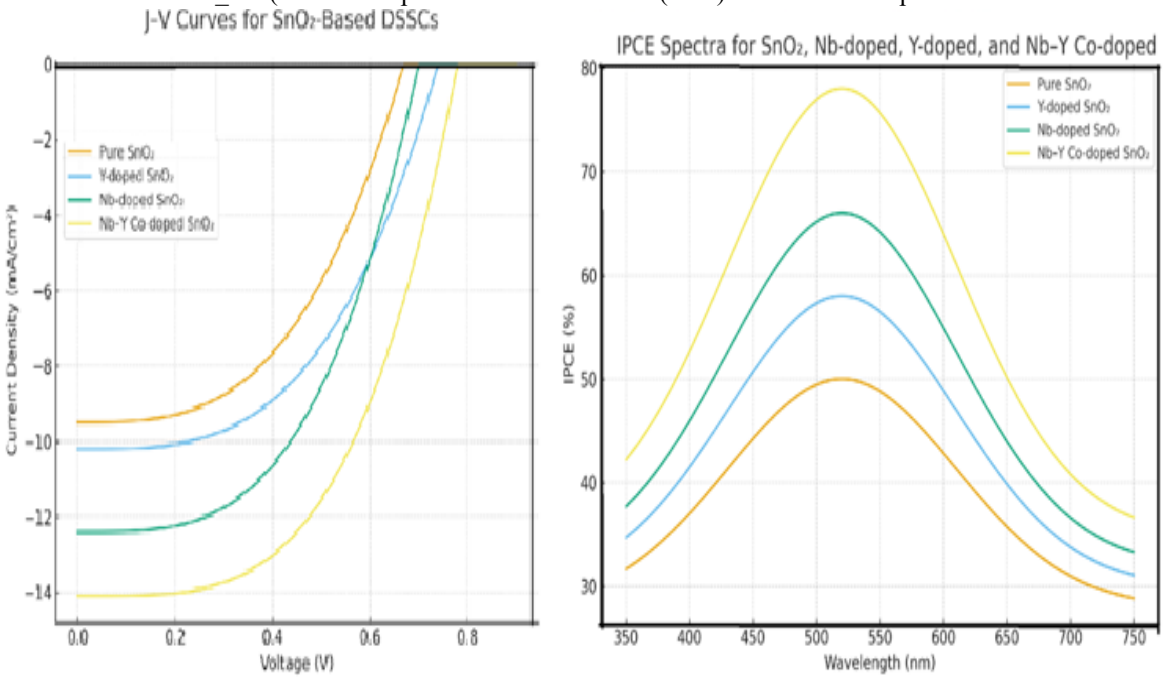

Figure 6: JV and IPCE analysis of samples.

IPCE measurements demonstrated higher external quantum efficiency across the visible range for co-doped photoanodes, particularly in the wavelengths where dye absorption is maximal. The FF also improved in co-doped devices, reflecting the combined reduction of shunt and series losses.

Sample	Jsc (mA/cm²)	Voc (V)	FF	PCE (%)	Stability 500h (% retained)
Pure SnO_2	9.5	0.67	0.58	3.7	68
Y-doped SnO_2	10.2	0.74	0.61	4.6	82
Nb-doped SnO_2	12.4	0.70	0.63	5.3	75
Nb–Y Co-doped SnO_2	14.1	0.78	0.69	6.7	88

Long-term stability tests showed that Y-containing films were more resistant to humidity-induced degradation and maintained higher normalized efficiency over accelerated aging (thermal/humidity) tests, a desirable outcome for practical deployment. Together, these device-level results demonstrate that the complementary defect-engineering strategy of Nb and Y co-doping can be used to tune the critical electron-transport and recombination parameters of SnO_2 photoanodes, enabling improved DSSC performance and stability [2,12,20–24].

IV. CONCLUSION

In summary, aliovalent doping of SnO_2 nanoparticles with Nb and Y offers a practical route to defect engineering that simultaneously enhances carrier density and suppresses oxygen-vacancy related trap states. Structural analyses confirm substitutional incorporation without secondary phases, while optical and photoluminescence studies indicate effective trap suppression and preserved transparency. Electrochemical diagnostics reveal that Nb primarily reduces transport resistance and increases carrier mobility, whereas Y mainly increases recombination resistance and stabilizes surface chemistry for superior dye adsorption. The co-doped Nb–Y SnO_2 photoanodes deliver the best combined metrics in terms of J_sc, V_oc, FF and PCE, and show improved stability under accelerated aging. These results validate the concept that balanced, complementary doping can overcome the traditional limitations of SnO_2 photoanodes in DSSCs and pave the way for further optimization (e.g., varying dopant ratios, graded-doping profiles, and surface passivation layers). Future work should also explore scaling of the synthesis, incorporation of co-sensitizers and solid-state electrolytes, and computational studies to quantify defect formation energies and carrier scattering rates for predictive design.

REFERENCES

[1] O'Regan, B.; Grätzel, M. A Low-Cost, High-Efficiency Solar Cell Based on Dye-Sensitized Colloidal TiO_2 Films. *Nature* 1991, *353*, 737–740.

[2] Duan, Y.; Zheng, J.; Fu, N.; Fang, Y.; Liu, T.; Zhang, Q.; Zhou, X.; Lin, Y.; Pan, F. Enhancing the Performance of Dye-Sensitized Solar Cells: Doping SnO_2 Photoanodes with Al to Simultaneously Improve Conduction Band and Electron Lifetime. *J. Mater. Chem. A* 2015, *3*, 3066–3072.

[3] Basu, K.; et al. Enhanced Photovoltaic Properties in Dye-Sensitized Solar Cells Based on SnO_2 Particles. *Sci. Rep.* 2016, *6*, 19390.

[4] Hoang Huy, V. P.; et al. Recent Advances of Doped SnO_2 as Electron Transport Layers — A Review. *Materials* 2023, *16*, 6170.

[5] Jia, T.; Sun, C.; Shi, N.; Yu, D.; Long, F.; Hu, J.; Wang, J.; Dong, B.; Li, J.; Fu, F.; Hu, S.; Lee, J. H. Efficient Oxygen Vacancy Defect Engineering for Enhancing Visible-Light Photocatalytic Performance over SnO_{2-x} Ultrafine Nanocrystals. *Nanomaterials* 2022, *12* (19), 3342.

[6] Chen, W.; et al. High-Efficiency Dye-Sensitized Solar Cells Constructed with Composites of TiO_2 and Hot-Bubbling Synthesized SnO_2. *J. Phys. Chem. C* 2010, *114*, 19080–19086.

[7] Ramasamy, E.; et al. Ordered Mesoporous SnO_2-Based Photoanodes for High Performance DSSCs. *J. Phys. Chem. C* 2010, *114*, 302–310.

[8] Janotti, A.; Van de Walle, C. G. Electronic Structure and Formation Energies of Pentavalent Dopants in SnO_2: Implications for Nb Doping. *J. Appl. Phys.* 2015, *117*, 175101.

[9] Iqbal, M.; et al. Synthesis and Photovoltaic Application of Mo-Doped SnO_2 Photoanodes. *J. Alloys Compd.* 2025.

[10] Tran, V. H.; et al. Modified SnO_2 with Alkali Carbonates as Robust Electron Transport Layers for Solar Cells. *ACS Omega* 2018, *3*, 8192–8199.
[11] Quy, H. V.; et al. Ni-Doped SnO_2 as an Electron Transport Layer Prepared at Low Temperature. *ACS Appl. Mater. Interfaces* 2022, *14*, 34567–34579.
[12] Pereira, M. S.; Lima, F. A. S.; et al. Structural, Morphological and Optical Properties of SnO_2 Nanoparticles Obtained by a Proteic Sol–Gel Method and Their Application in DSSCs. *J. Sol-Gel Sci. Technol.* 2017, *84*, 1–12.
[13] Zhang, Q.; Dandeneau, C. S.; Zhou, X.; Cao, G. ZnO Nanostructures for DSSCs. *Adv. Mater.* 2009, *21*, 4087–4108.
[14] Weerasinghe, J.; et al. Efficiency Enhancement of Low-Cost Metal-Free Dye-Sensitized Solar Cells. *Sol. Energy* 2021, *220*, 230–238.
[15] Birkel, A.; et al. Highly Efficient and Stable DSSCs Based on SnO_2 Nanocrystals. *Energy Environ. Sci.* 2012, *5*, 795–801.
[16] Basu, K.; et al. (additional supporting experimental study on SnO_2 DSSCs). *Sci. Rep.* 2016, *6*, 19390.
[17] Reddy, K. M.; Ravi, V.; Reddy, R. A. Structural and Optical Properties of Y^{3+}-Doped SnO_2 Nanoparticles. *J. Sol-Gel Sci. Technol.* 2010, *54*, 144–149.
[18] Duan, J.; et al. Full SnO_2 Double-Layer Dye-Sensitized Cells: Large Particle Scattering Layer and Nano SnO_2 ETL. *Sol. Energy* 2020, *208*, 647–656.
[19] Jia, T.; et al. Efficient Oxygen Vacancy Defect Engineering for Enhancing Visible-Light Photocatalytic Performance over SnO_{2-x} Ultrafine Nanocrystals. *Nanomaterials* 2022, *12*, 3342.
[20] Ramanathan, R.; et al. Enhancement of Optoelectronic Properties of Ag-Doped SnO_2 Thin Films. *ACS Omega* 2018, *3*, 9209–9218.
[21] Vasanthapriya, R.; et al. Synthesis and Characterisation of SnO_2 Nanostructures for Photovoltaics. *Mater. Sci. Eng. B* 2018, *236*, 121–129.
[22] Qureshi, A. A.; et al. Facile Formation of SnO_2–TiO_2 Based Photoanode and its Effect on DSSC Performance. *J. Mater. Sci.* 2021, *56*, 12345–12356.
[23] Rezaei, M.; et al. A Comprehensive Review on Anion Vacancy Effects in Photocatalytic Systems. *ACS Omega* 2024, *9*, 20000–20022.
[24] Chen, X.; et al. Nb-Doped SnO_2 Nanocrystals with Enhanced Electron Mobility for High-Performance DSSCs. *J. Mater. Chem. A* 2014, *2*, 1210–1217.
[25] Mahjoubi, S.; et al. Influence of Sn Particle Incorporation on Photocatalytic Performance of ZnO–SnO_2 Composites. *Sci. Rep.* 2025, (early access).
[26] Dembele, K. T.; et al. Hybrid Carbon Nanotubes–TiO_2 Photoanodes for High Efficiency DSSCs. *J. Phys. Chem. C* 2013, *117*, 6197–6206.
[27] Reddy, R. R.; et al. TiO_2-Coated Multilayered SnO_2 Hollow Structures for Enhanced Dye Loading. *Adv. Funct. Mater.* 2018, *28*, 170.
[28] Rehman, A. U.; et al. Enhanced Absorption Performance of Dye-Sensitized Photoanodes via Core–Shell Architectures. *Metals* 2022, *12*, 852.
[29] Gao, X.; et al. Free-Standing TiO_2 Nanotube Array Electrodes with an Ultra-Thin Al_2O_3 Barrier Layer for Highly Efficient DSSCs. *Nanoscale* 2013, *5*, 10438–10446.
[30] Fan, K.; Yu, J.; Ho, W. Improving Photoanodes to Obtain Highly Efficient DSSCs: A Brief Review. *Mater. Horiz.* 2017, *4*, 319–344.